



ВНИИА
РОСАТОМ

From **low-intensity** exposures for photonics and optoacoustics to **intense** ultrashort hard X-rays

Zababakhin Scientific Talks 2025

Inogamov Nail' Alimovich

Main Scientific Researcher, Dukhov Automatics Research Institute

21.05.2025

The world of lasers

Wavelength – Energy – Duration

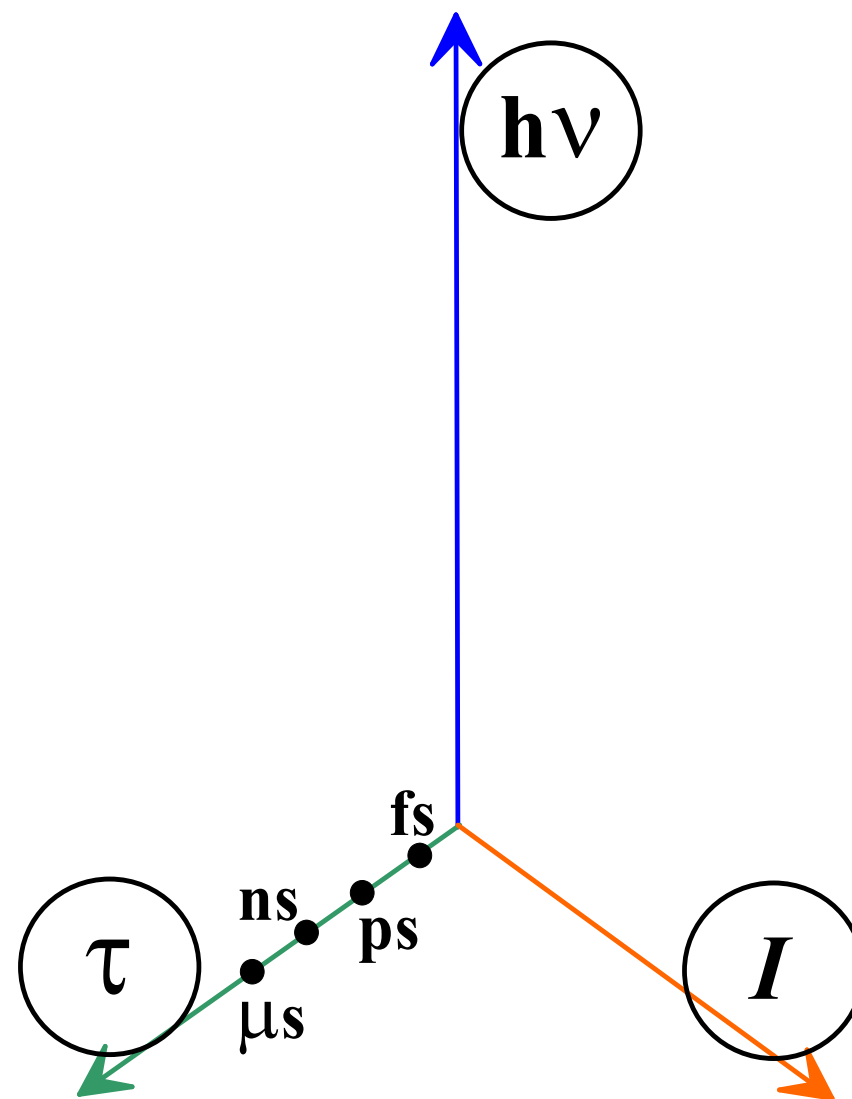
*This 3D volume is densely populated
by very diverse laser systems*

photon characteristics

$$\lambda - \nu - h\nu$$

energy characteristics

$$I - F = I * \tau - E = F * S$$

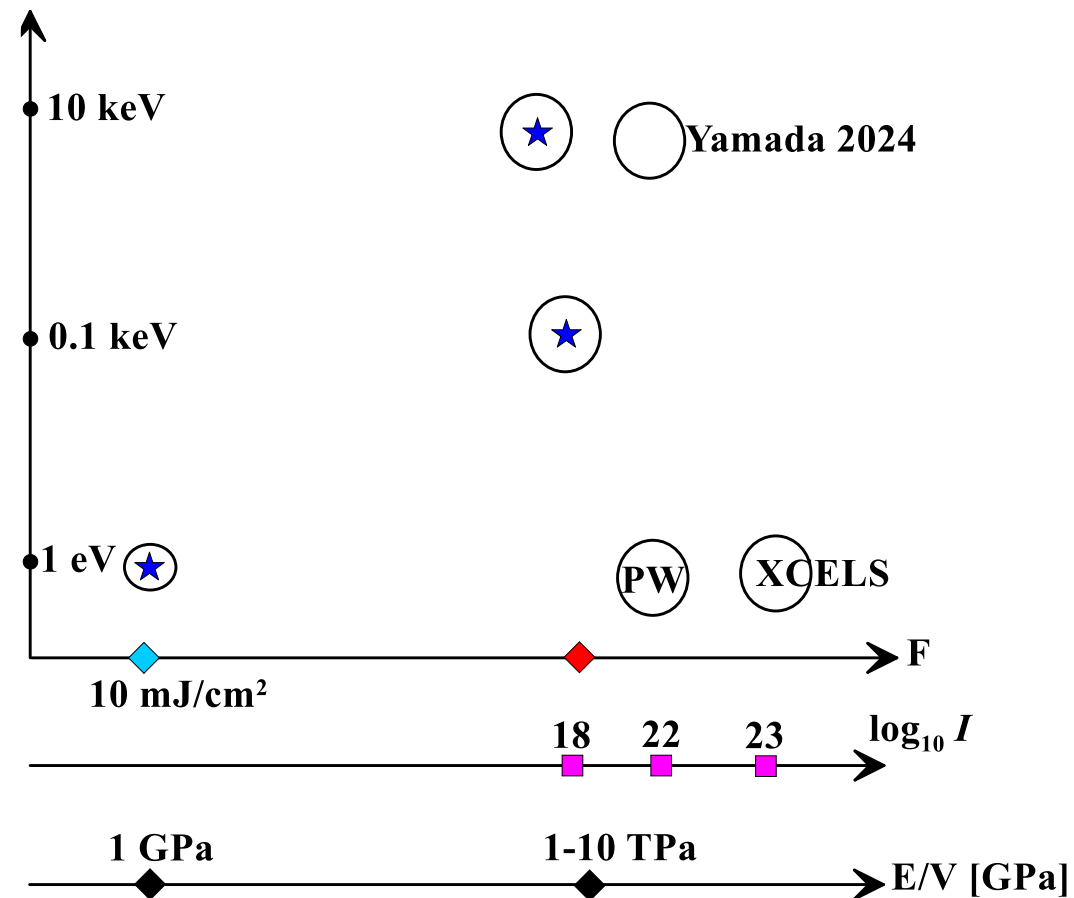


The world of lasers

Wavelength – Energy. Duration =fs-ps

In this talk I consider ultrashort laser pulses = fs-ps range of durations.

To the right is a map illustrating the world of fs-ps lasers.



XCELS=eXawatt Center for Extreme Light Studies

Yamada, J. *et al.* Extreme focusing of hard XFEL.. **7 nm focus** .. 10²² W cm⁻² intensity. *Nat. Photonics* (2024)

The world of lasers

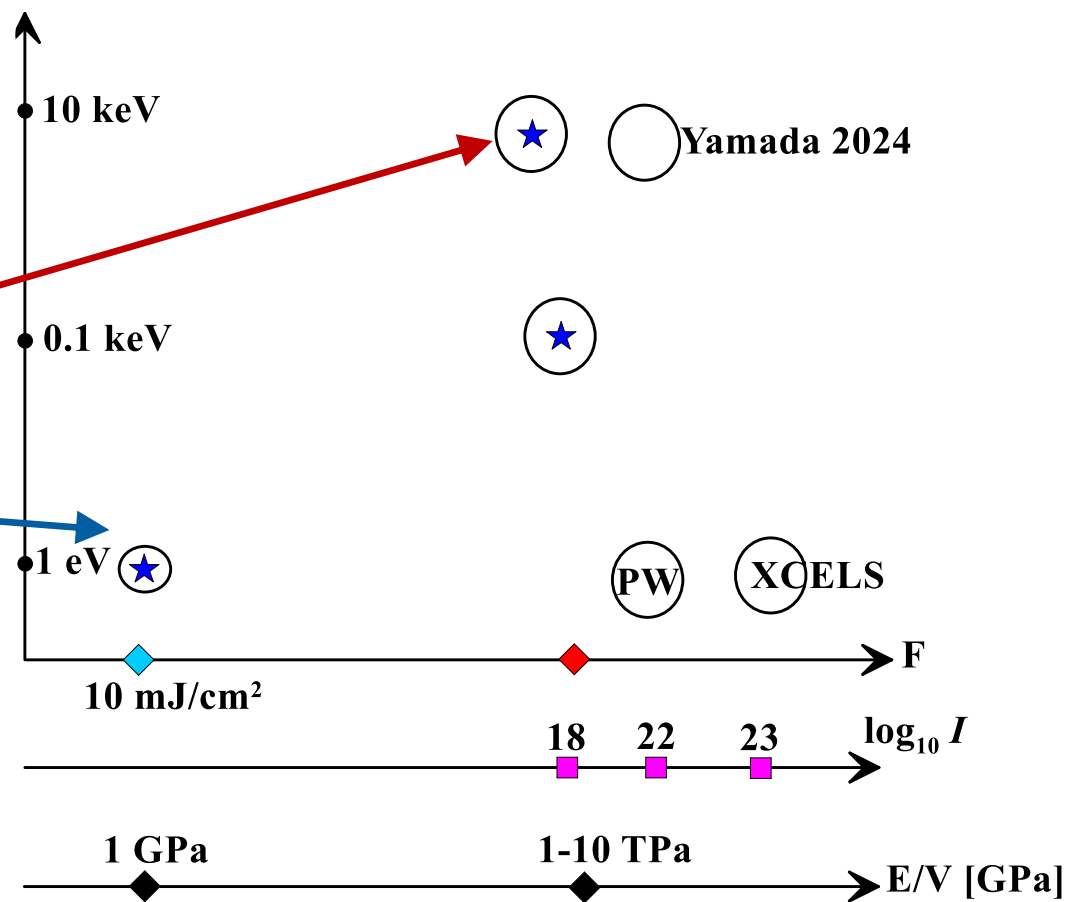
Wavelength – Energy. Duration =fs-ps

О чём речь

The purpose of the report is twofold

1) OptoAcoustics and NanoPhotonics

2) hard X-ray



NanoPhotonics and optoAcoustics

it's two **separate** large worlds

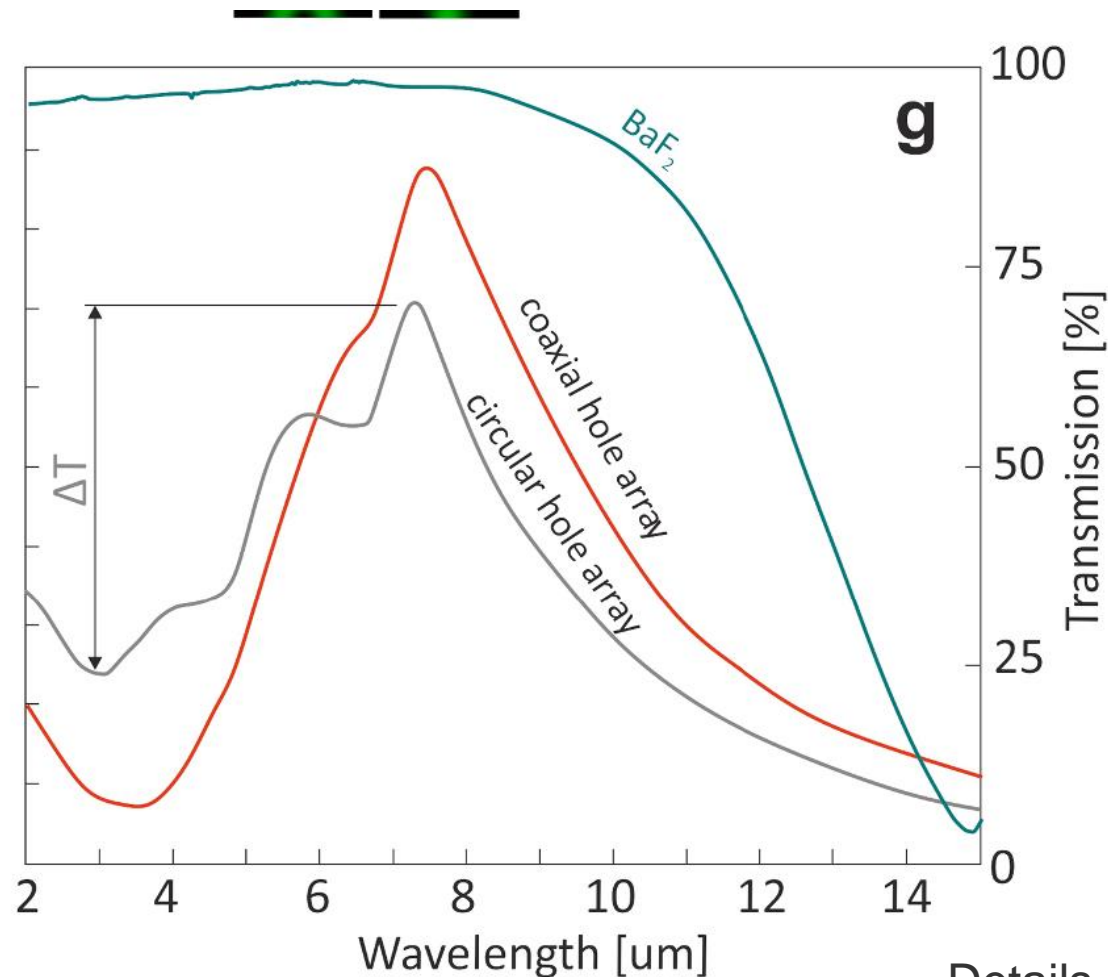
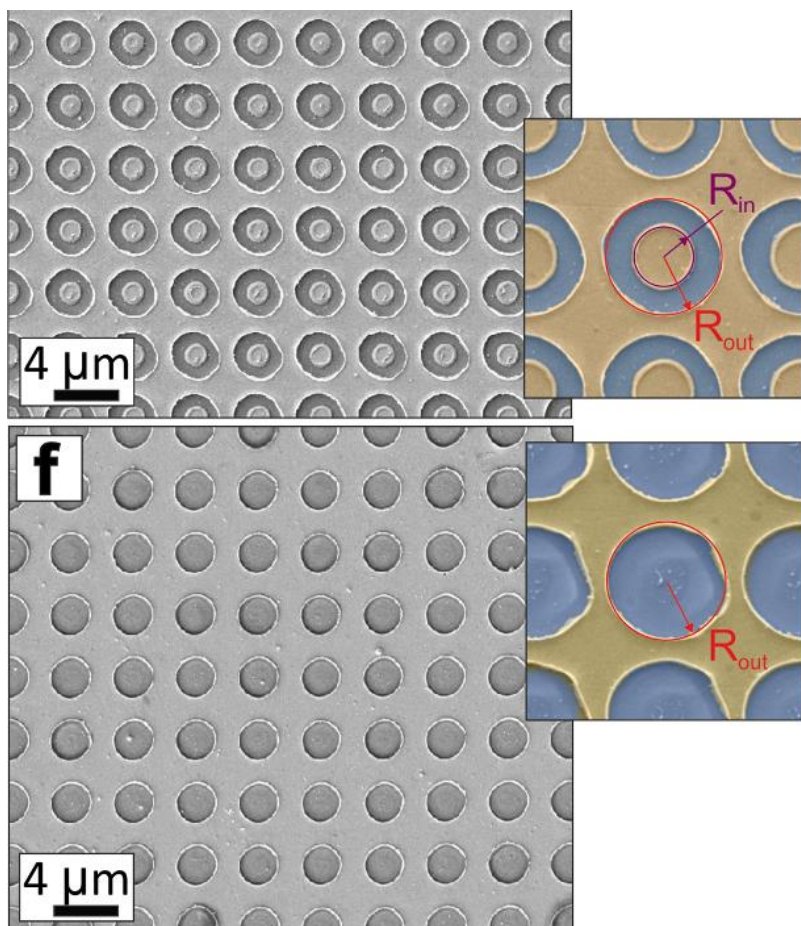
Photonics manipulates photons with metasurfaces.
The metasurfaces are stationary: **motionless**

In optoacoustics, light thermo-mechanically **moves** the target substance

This is probably the first time in our work that the motion of matter affects light manipulation.

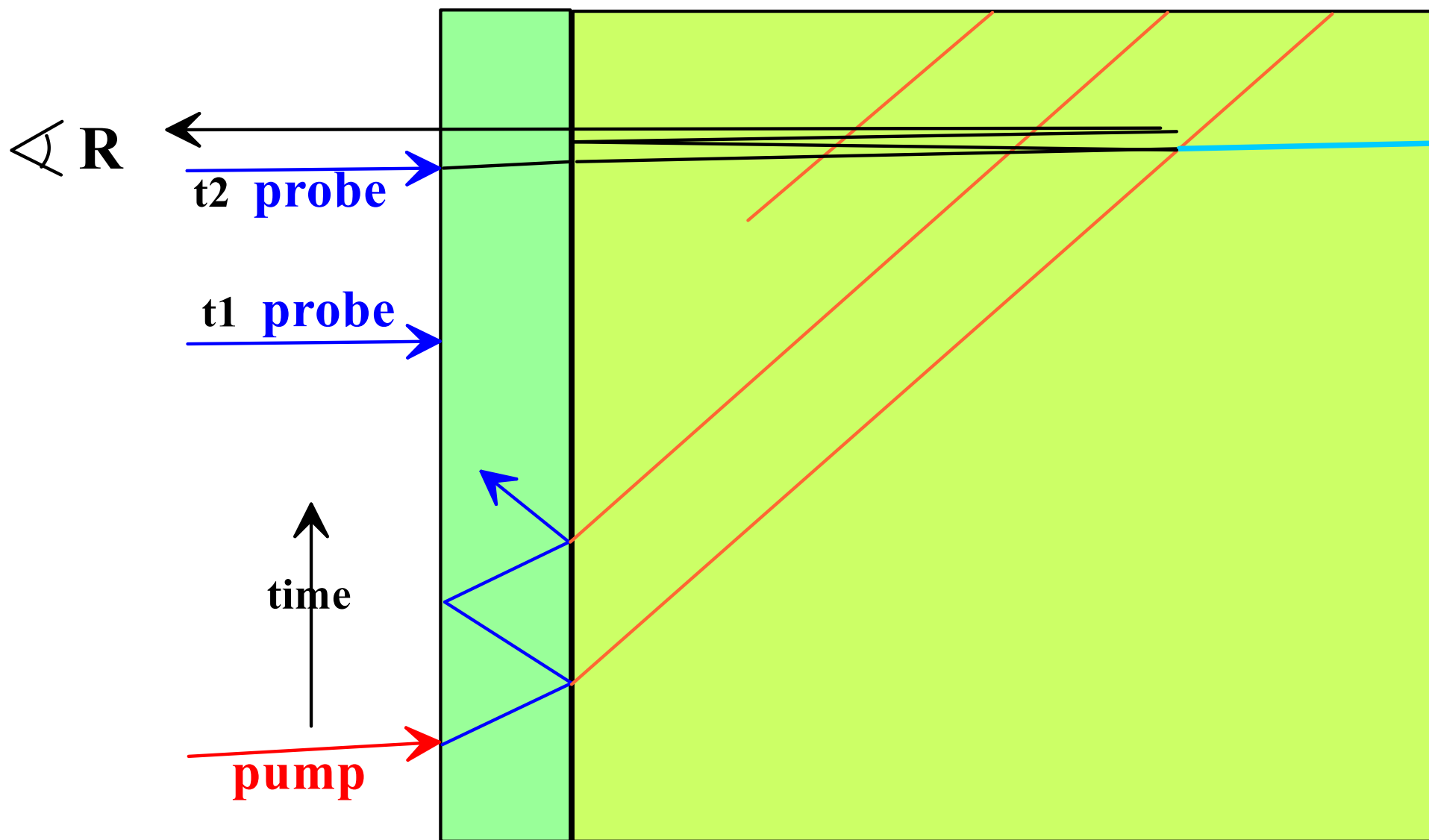
We excite acoustic phenomena in metasurfaces designed **for photonics.**

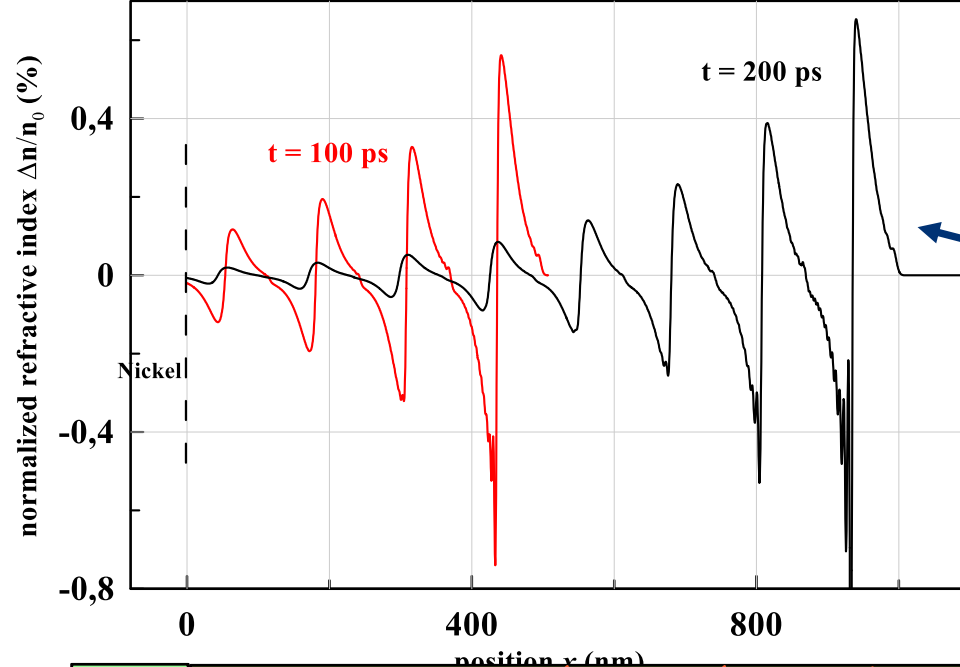
NanoPhotonics



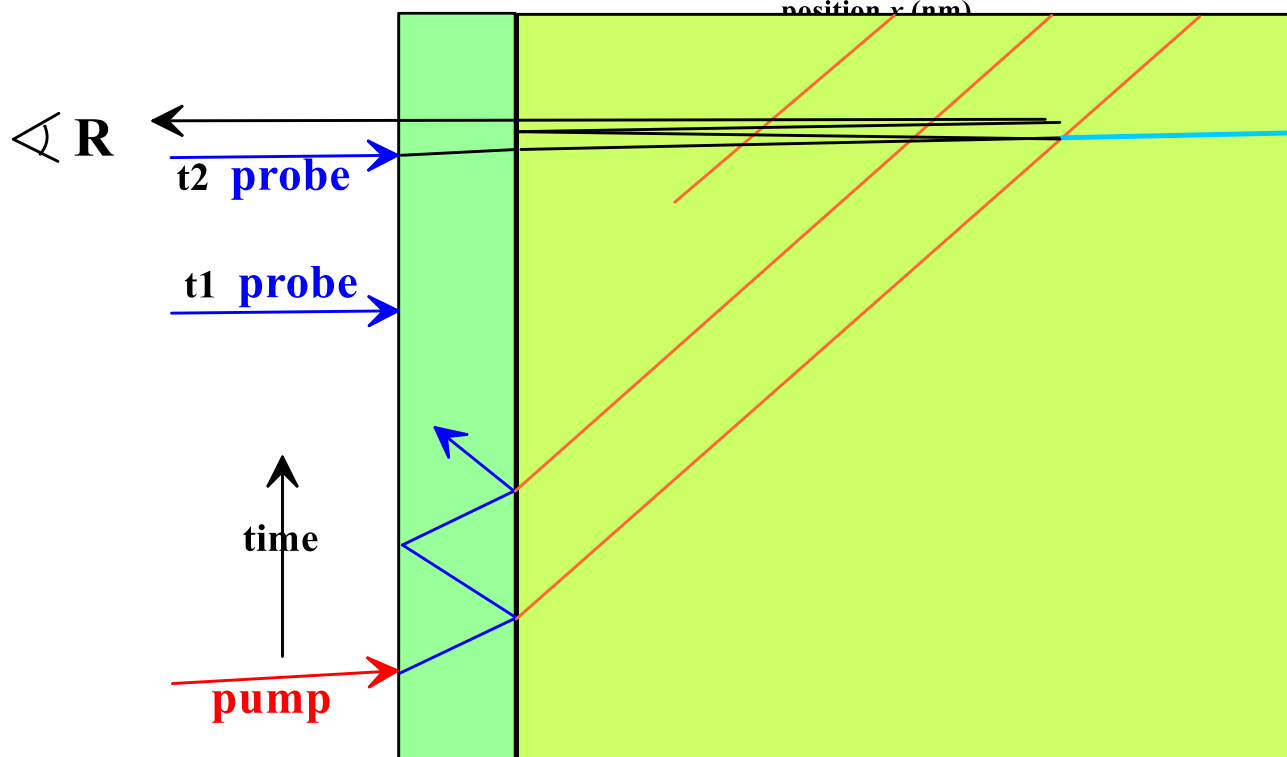
Details of the array
modifies
transmission and
reflection.
The array is
metasurface

Velocity of light is very high:
5 orders of magnitude above speed of sound.
Thus, every probe illuminating the device at the instant t_i
gives us reflectivity R of a film skin+ acoustic wave in glass
at the instant t_i .

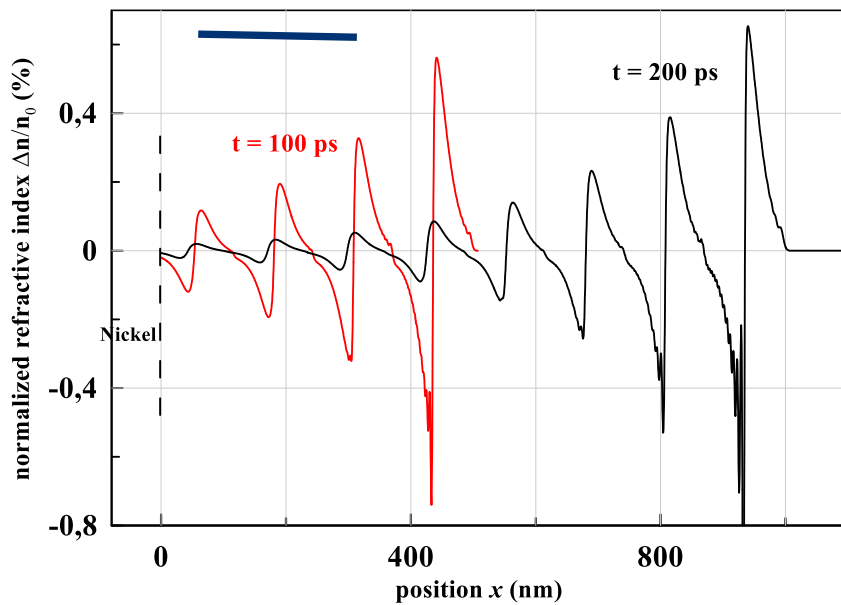




The profiles of the acoustic wave are shown for the instants t_1 and t_2 of illumination by probes

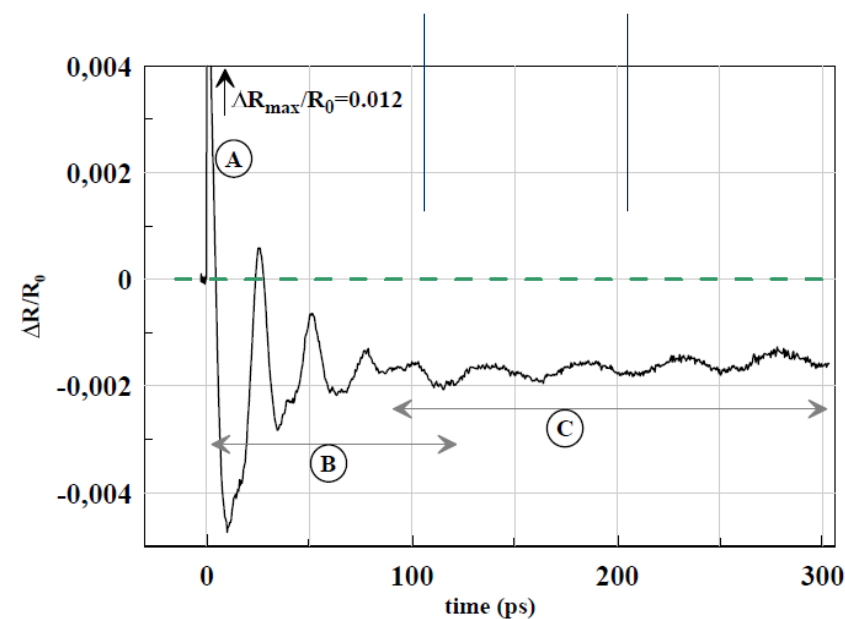
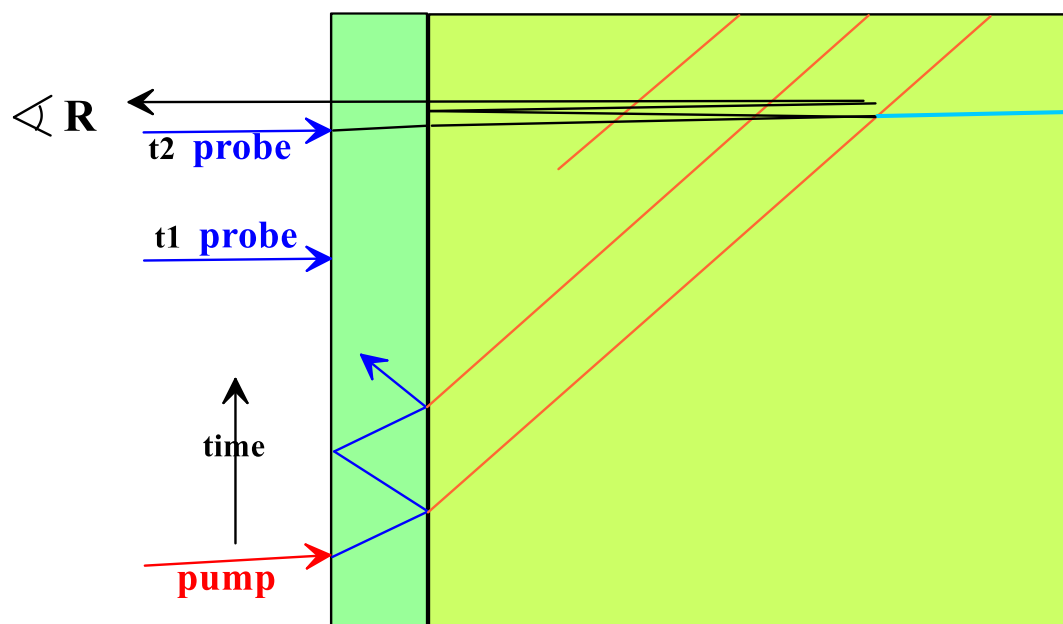


Probe light shines through and reflects (1) from skin in Ni + (2) from refractive index changes of the acoustic wave

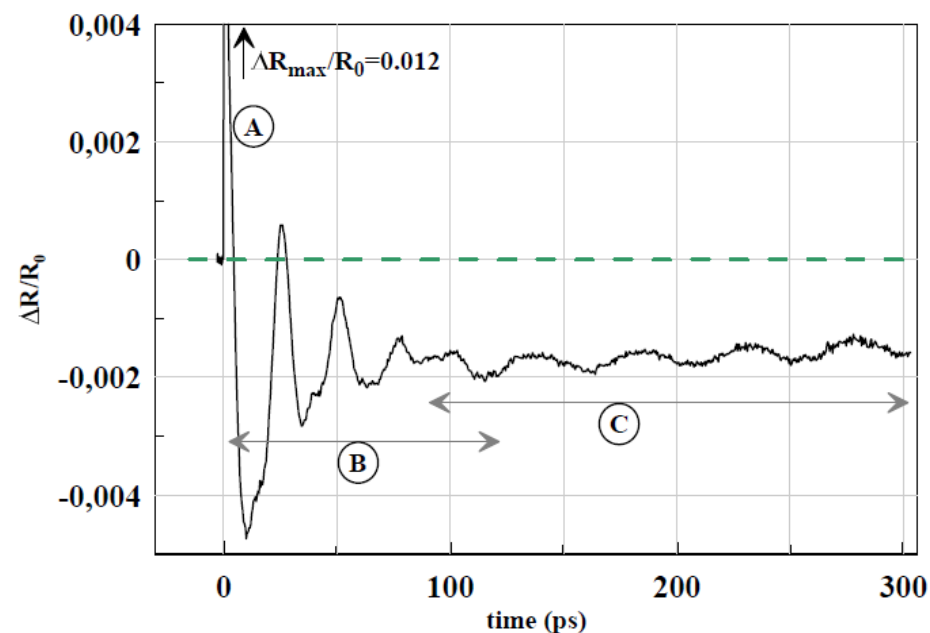
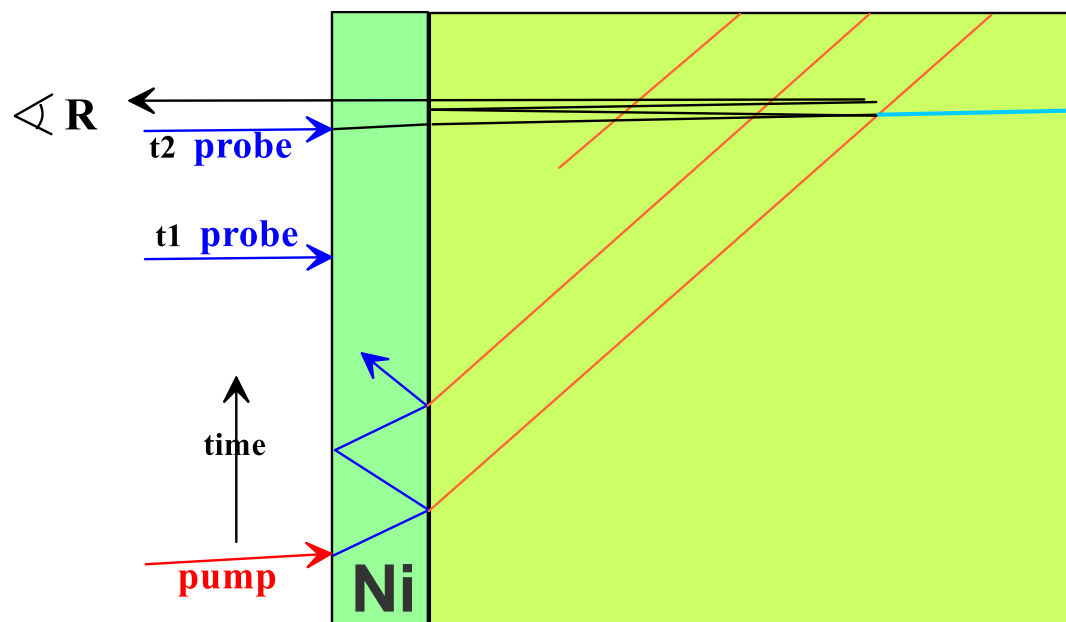


$R_0 \sim 0.4$ (mainly from skin)
 ΔR from optoAc perturbations $\sim 10^{-4}$

Lock-in = synchronous detection



$$L_B = \lambda/2/n$$



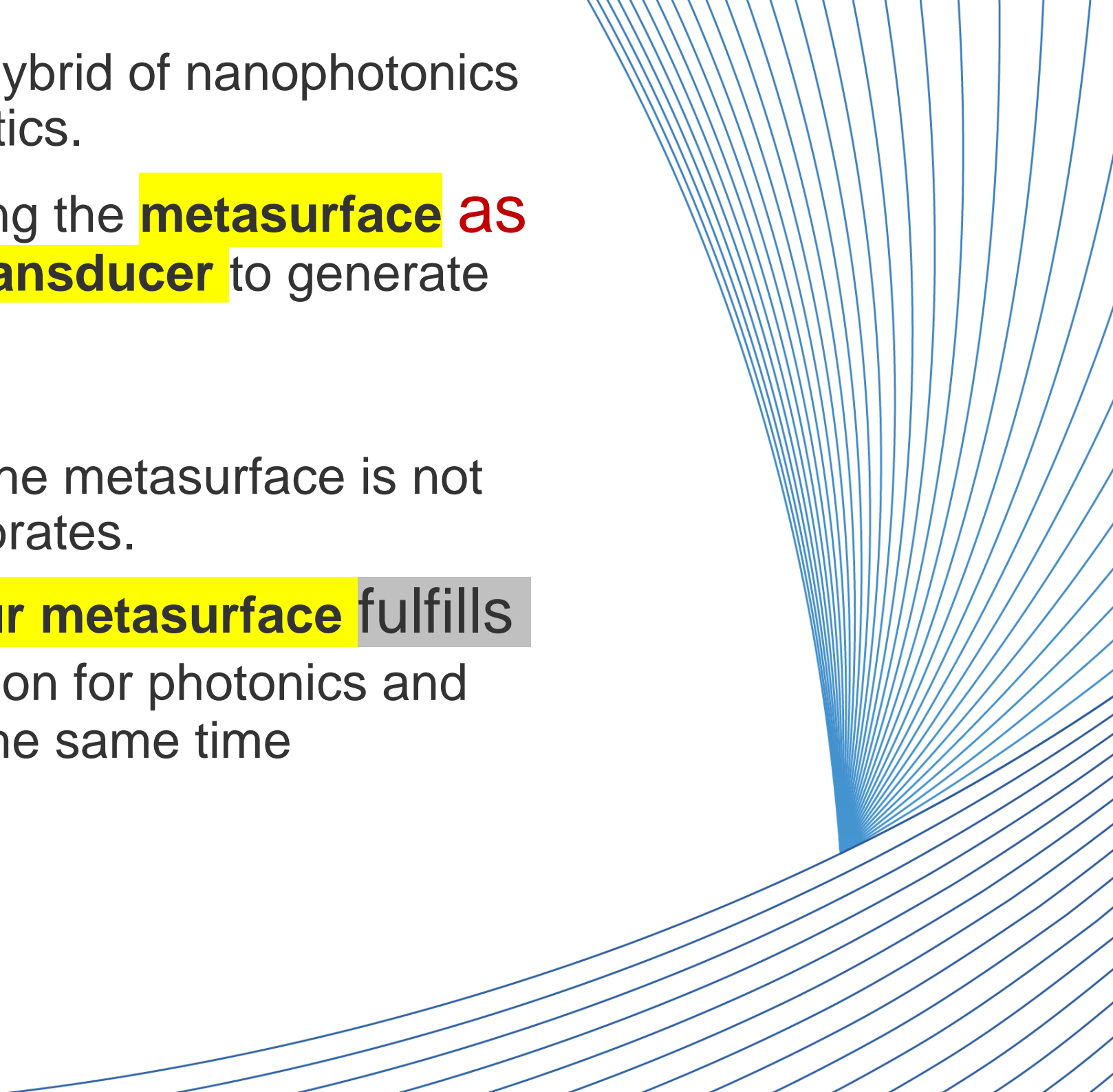
Above the slides explained the principle of optoacoustics in our device.
Where is the photonics in this?

To see “Brillouin” through a metal film, the thickness of the film “ df ” must be less than the thickness of the skin layer. But then Brillouin oscillations will have a very high frequency of $2\text{ cs}/df$.

To control the frequency of the Brillouin oscillations one needs geometrically thick films. But such films will be optically thick and will not transmit light.

Output = film as a **metaFilm** = as a film with two metaSurfaces - as a photonic surface

- We created a hybrid of nanophotonics and optoacoustics.
- We started using the **metasurface** as an **acoustic transducer** to generate sound
- In our device, the metasurface is not stationary, it vibrates.
- In this case, **our metasurface** fulfills **both** the function for photonics and transducer at the same time



MetaFilm

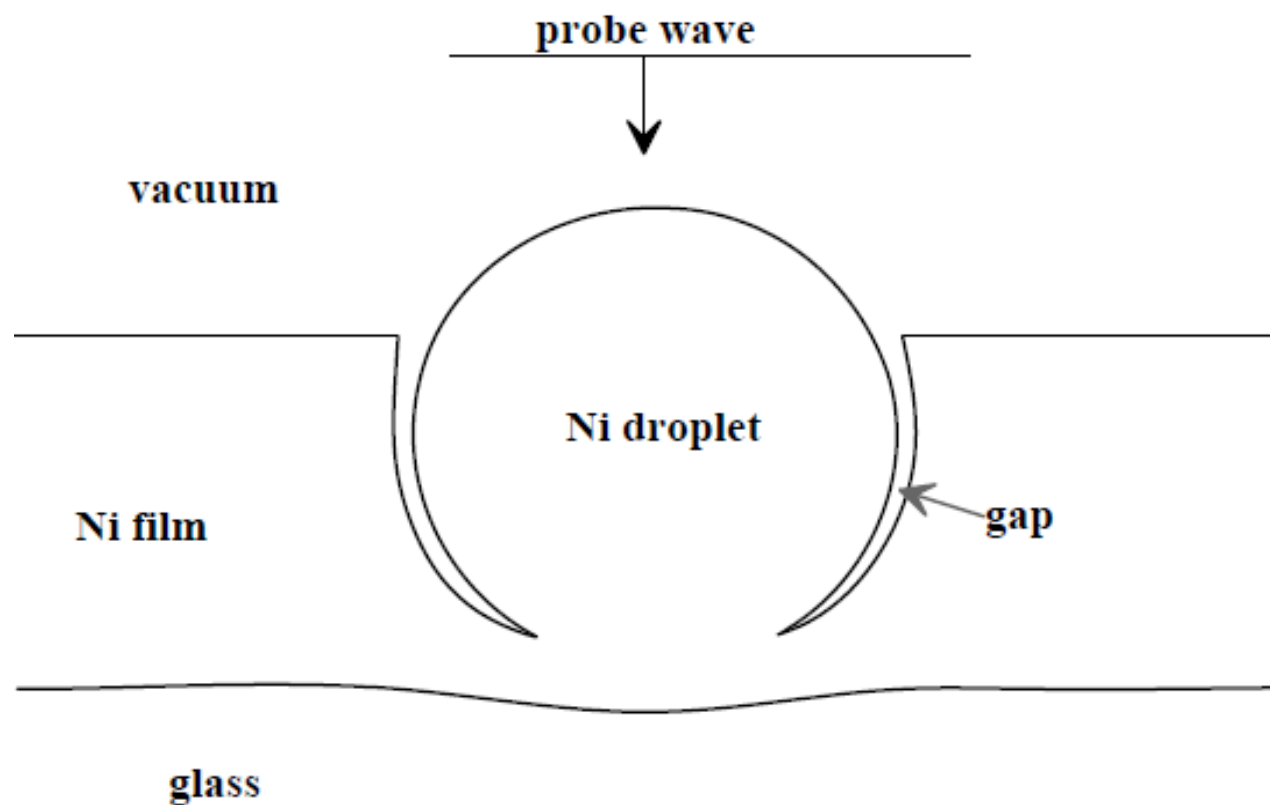
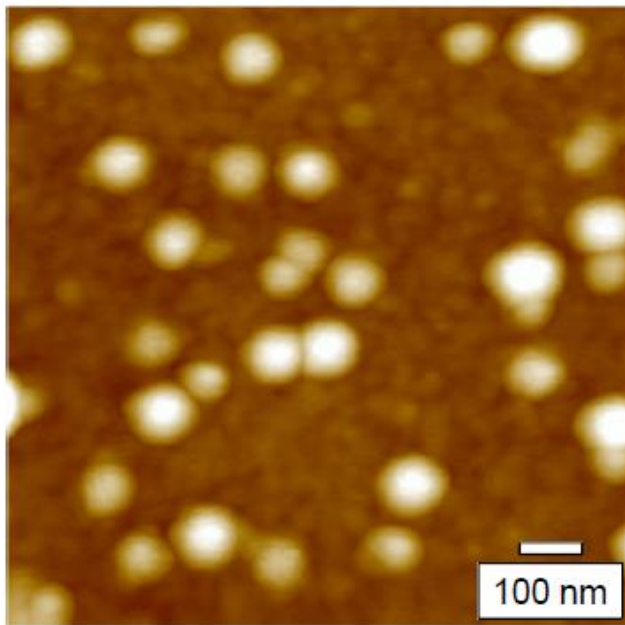


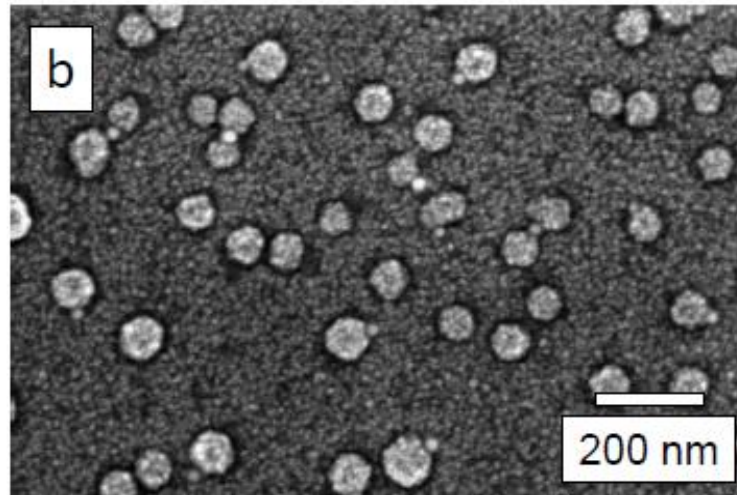
Рис. 1. Пленка никеля (Ni film) с шаровидным включением (Ni droplet) на стеклянной подложке (glass). Наночар диаметром 50-70 нм окружен зазорами (gap) вокруг.

MetaFilm

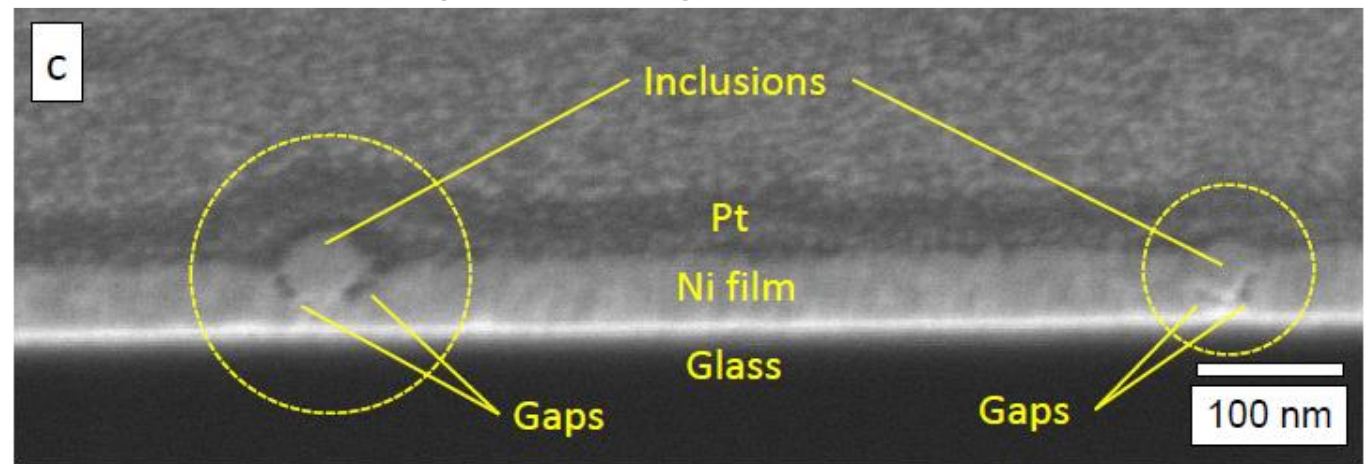
AFM image



SEM image



FIB cutting + SEM image of the cut

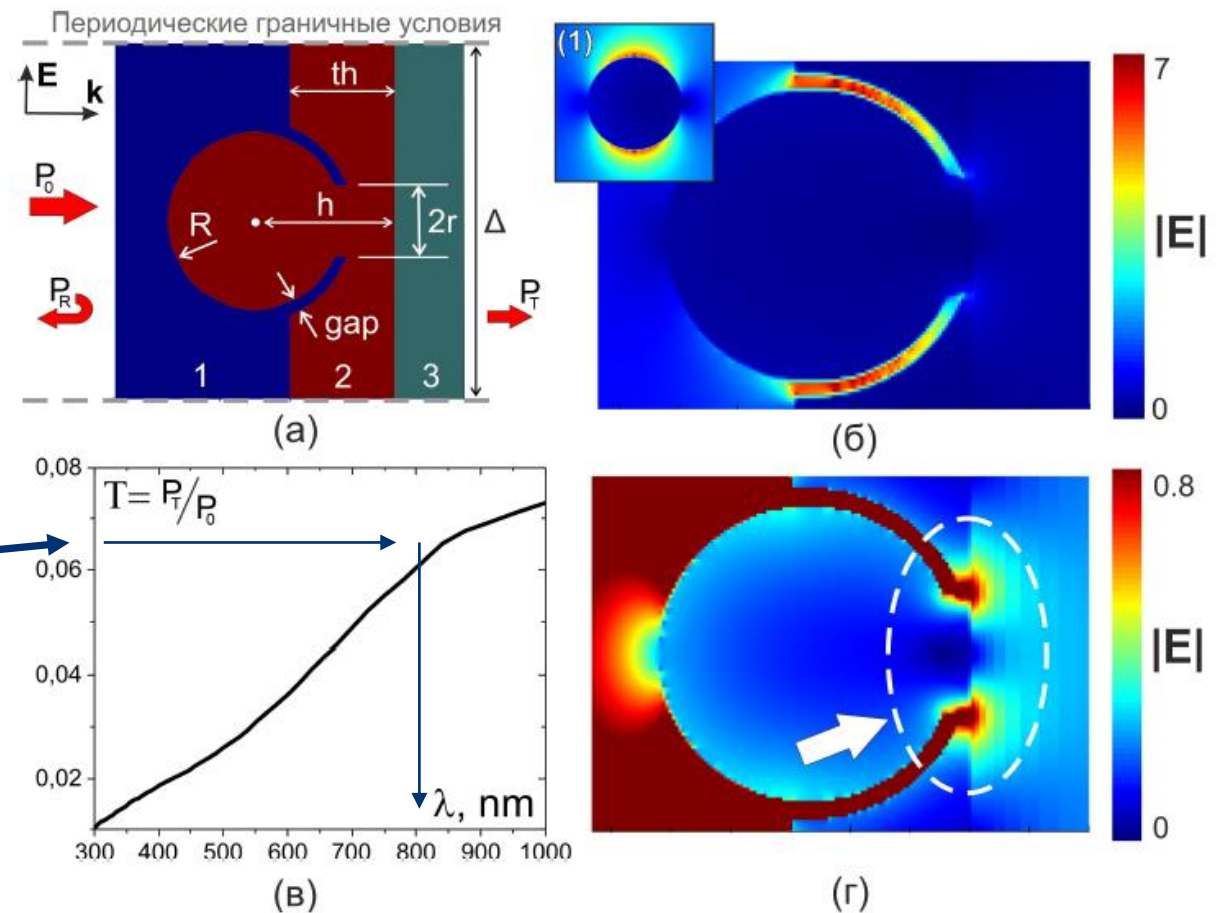


Plasmonics of our MetaFilm

2-3 orders of magnitude enhancement of transmitting of light through optically thick Nickel film

Optically thick means = geometrical thickness $df = 70 \text{ nm}$
Skin depth $dSk = 13 \text{ nm}$

$\text{Exp}(2 df/dSk) = 50\,000 = 50 \text{ thousands,}$
 $1/50000 = 0.2 \cdot 10^{-4}$
versus Transmittance = 0.07



Formation of high-aspect-ratio nanocavity in LiF crystal using a femtosecond of x-ray FEL pulse

Sergey S. Makarov,*¹ Sergey A. Grigoryev,¹ Vasily V. Zhakhovsky,¹ Petr Chuprov,² Tatiana A. Pikuz,³ Nail A. Inogamov,^{1,4} Victor V. Khokhlov,^{1,4} Yuri V. Petrov⁴, Eugene Perov,¹ Vadim Shepelev,² Takehisa Shobu,⁵ Aki Tominaga,⁵ Ludovic Rapp,⁶ Andrei V. Rode,⁶ Saulius Juodkazis^{7,8}, Mikako Makita,⁹ Motoaki Nakatsutsumi,⁹ Thomas R. Preston,⁹ Karen Appel,⁹ Zuzana Konopkova,⁹ Valerio Cerantola,^{9,10} Erik Brambrink,⁹ Jan-Patrick Schwinkendorf,⁹ István Mohácsi,⁹ Vojtech Vozda,¹¹ Vera Hajkova,¹¹ Tomas Burian,¹¹ Jaromir Chalupsky¹¹, Libor Juha,¹¹ Norimasa Ozaki¹², Ryosuke Kodama^{12,13}, Ulf Zastra⁹ and Sergey A. Pikuz¹⁴

¹Joint Institute for High Temperatures of Russian Academy of Sciences, 13/2 Izhorskaya st., 125412 Moscow, Russia.

²Institute for Computer Aided Design, Russian Academy of Sciences, Moscow, 123056 Russia.

³Institute for Open and Transdisciplinary Research Initiatives, Osaka University, Suita, 565-0871, Osaka, Japan.

⁴Landau Institute for Theoretical Physics of Russian Academy of Sciences, 1-A Akademika Semenova av., Chernogolovka, Moscow Region, 142432, Russia.

⁵The facility is Material Science Research Center, Japan Atomic Energy Agency, Sayo, Hyogo 679-5148, Japan.

⁶Laser Physics Centre, Department of Quantum Science and Technology, Research School of Physics, Australian National University, Canberra ACT 2600, Australia.

⁷Optical Sciences Centre and ARC Training Centre in Surface Engineering for Advanced Materials (SEAM), School of Science, Swinburne University of Technology, Melbourne, Australia.

⁸Tokyo Tech World Research Hub Initiative (WRHI), School of Materials and Chemical Technology, Tokyo Institute of Technology, Tokyo 152-8552, Japan.

⁹European XFEL, Holzkoppel 4, 22869 Hamburg, Germany.

¹⁰Università degli Studi di Milano Bicocca, Piazza della Scienza 4, 20126 Milano, Italy

¹¹Department of Radiation and Chemical Physics, Institute of Physics, Czech Academy of Sciences, Na Slovance 1999/2, 182 00 Prague 8, Czech Republic

¹²Graduate School of Engineering, Osaka University, Suita, 565-0871 Osaka, Japan

Formation of high-aspect-ratio nanocavity in LiF crystal using a femtosecond of x-ray FEL pulse

Sergey S. Makarov,*¹ Sergey A. Grigoryev,¹ Vasily V. Zhakhovsky,¹ Petr Chuprov,² Tatiana A. Pikuz,³ Nail A. Inogamov,^{1,4} Victor V. Khokhlov,^{1,4} Yuri V. Petrov⁴, Eugene Perov,¹ Vadim Shepelev,² Takehisa Shobu,⁵ Aki Tominaga,⁵ Ludovic Rapp,⁶ Andrei V. Rode,⁶ Saulius Juodkazis^{7,8}, Mikako Makita,⁹ Motoaki Nakatsutsumi,⁹ Thomas R. Preston,⁹ Karen Appel,⁹ Zuzana Konopkova,⁹ Valerio Cerantola,^{9,10} Erik Brambrink,⁹ Jan-Patrick Schwinkendorf,⁹ István Mohácsi,⁹ Vojtech Vozda,¹¹ Vera Hajkova,¹¹ Tomas Burian,¹¹ Jaromir Chalupsky¹¹, Libor Juha,¹¹ Norimasa Ozaki¹², Ryosuke Kodama^{12,13}, Ulf Zastra⁹ and Sergey A. Pikuz¹⁴

¹Joint Institute for High Temperatures of Russian Academy of Sciences, 13/2 Izhorskaya st., 125412 Moscow, Russia.

²Institute for Computer Aided Design, Russian Academy of Sciences, Moscow, 123056 Russia.

³Institute for Open and Transdisciplinary Research Initiatives, Osaka University, Suita, 565-0871, Osaka, Japan.

⁴Landau Institute for Theoretical Physics of Russian Academy of Sciences, 1-A Akademika Semenova av., Chernogolovka, Moscow Region, 142432, Russia.

⁵The facility is Material Science Research Center, Japan Atomic Energy Agency, Sayo, Hyogo 679-5148, Japan.

⁶Laser Physics Centre, Department of Quantum Science and Technology, Research School of Physics, Australian National University, Canberra ACT 2600, Australia.

⁷Optical Sciences Centre and ARC Training Centre in Surface Engineering for Advanced Materials (SEAM), School of Science, Swinburne University of Technology, Victoria 3122, Australia.

⁸Tokyo Tech World Research Hub Initiative (WRHI), School of Materials and Chemical Technology, Tokyo Institute of Technology, Tokyo 152-8552, Japan.

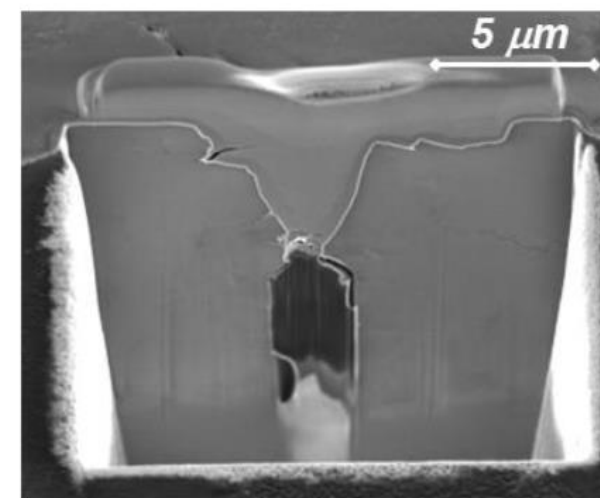
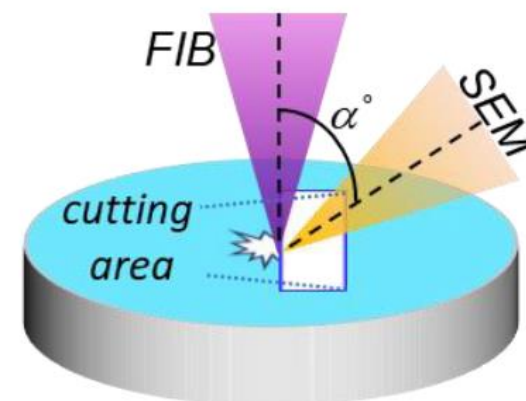
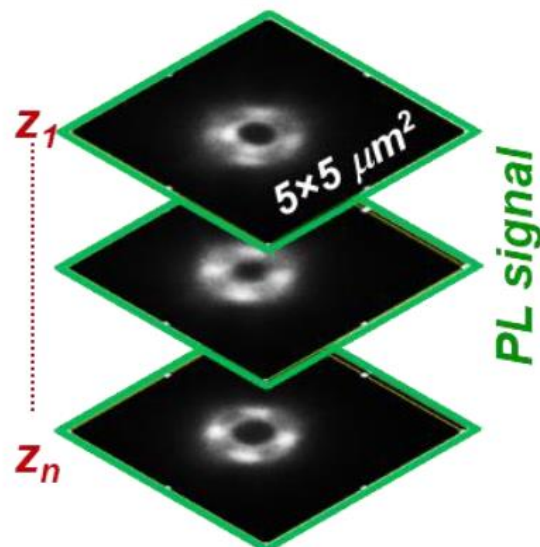
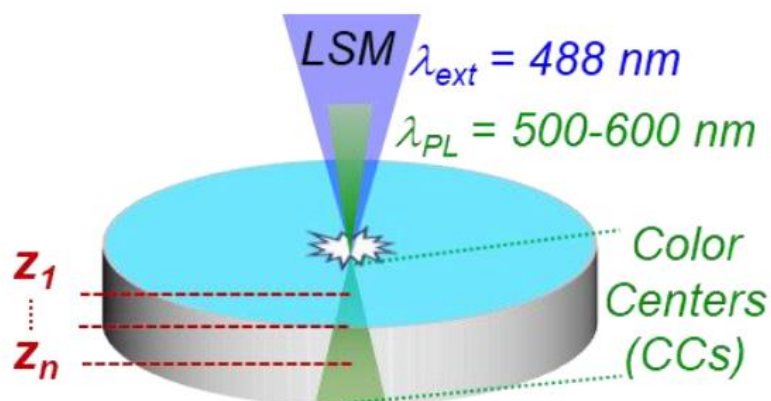
⁹European XFEL, Holzkoppel 4, 22869 Hamburg, Germany.

¹⁰Università degli Studi di Milano Bicocca, Piazza della Scienza 4, 20126 Milano, Italy

¹¹Department of Radiation and Chemical Physics, Institute of Physics, Czech Academy of Sciences, Na Slovance 1999/2, 182 00 Prague 8, Czech Republic

¹²Graduate School of Engineering, Osaka University, Suita, 565-0871 Osaka, Japan

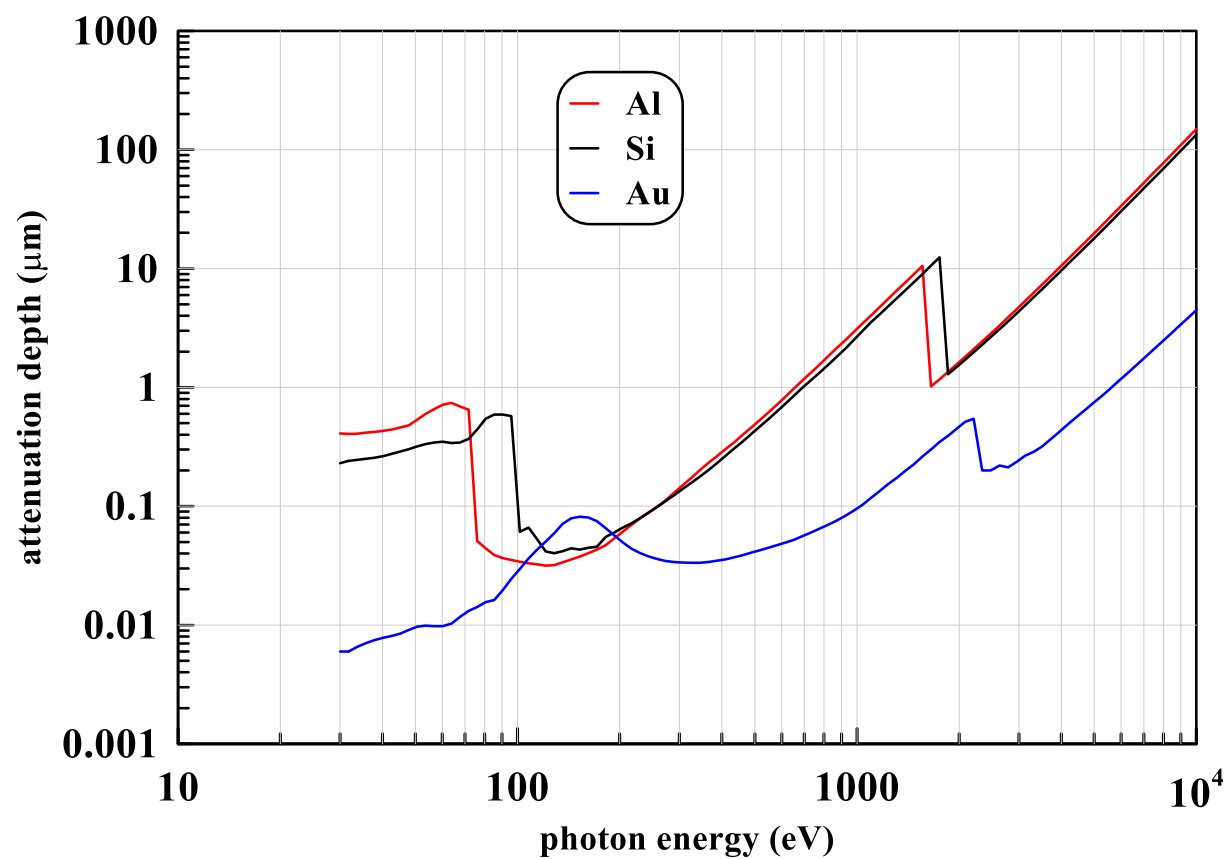
Techniques for analysing a 9 keV, 20 fs hard XFEL experiment are shown, energy density 1 MJ/cm³
 But now these huge energy density is distributed along long distance –
 much longer than in the case with soft X





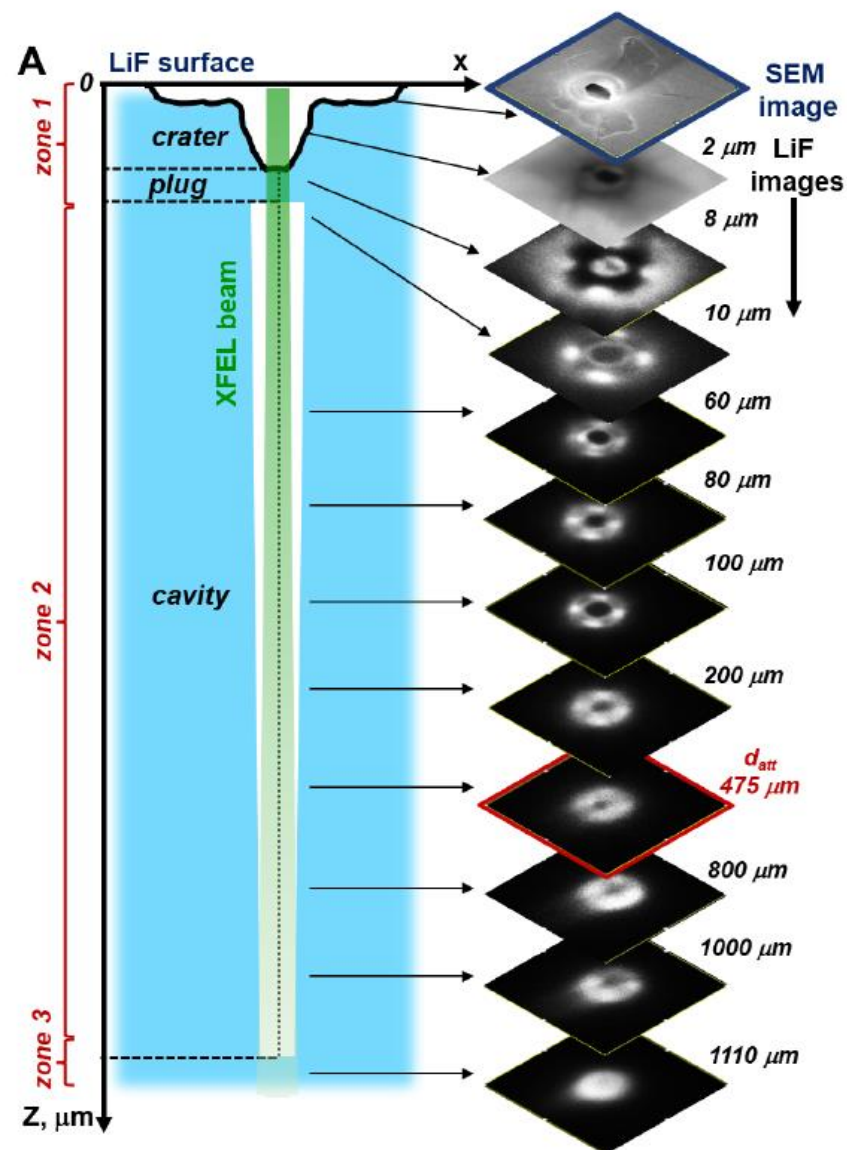
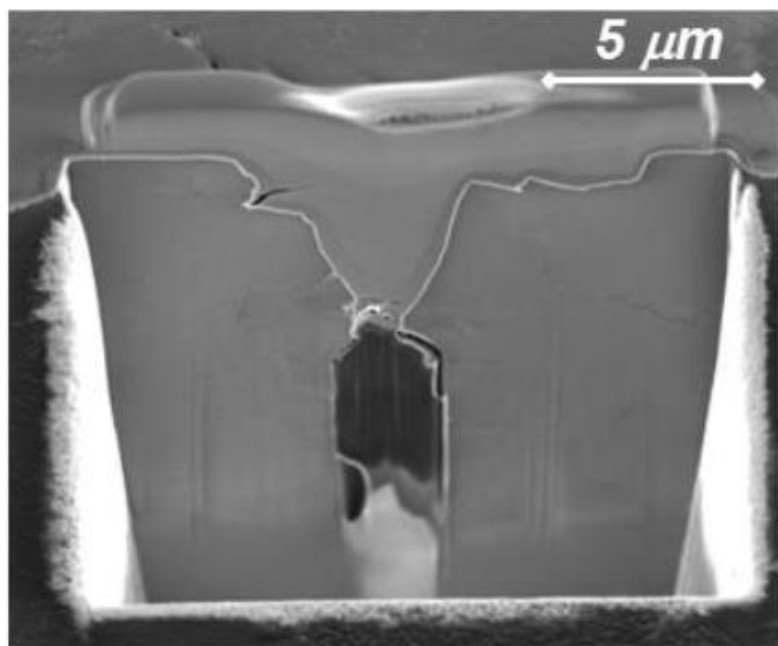
Gold	Al	Be	LiF
3.4 μm	110 μm	7.3 mm !	475 μm = 0.5 mm

Attenuation depth from Henke. Table data are for 9 keV



Three zones

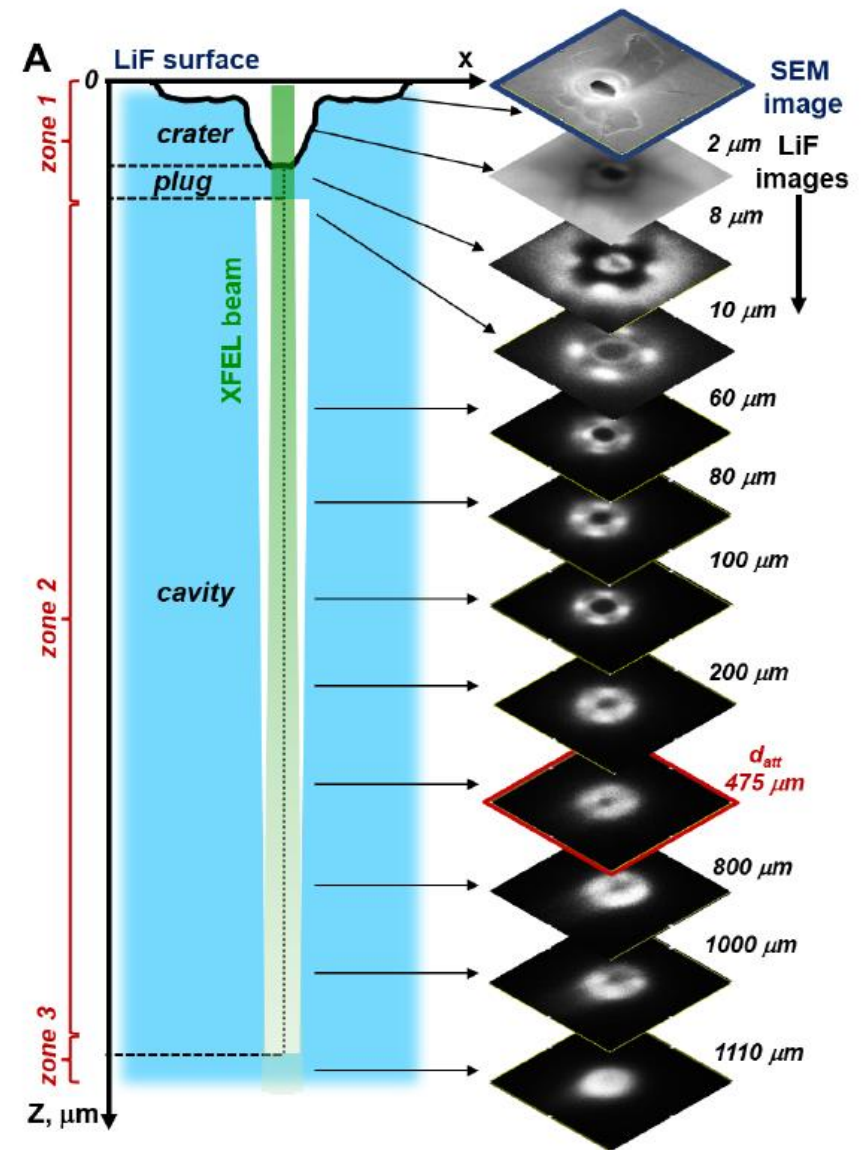
The first one is near surface
it is rather short
10-20 diameters



Three zones

The second one is in the middle, it is very long – up to 10^3 of the diameters.

Strong shock expanding in cylindrical radial direction causes radial extrusion of matter leaving behind empty cavity



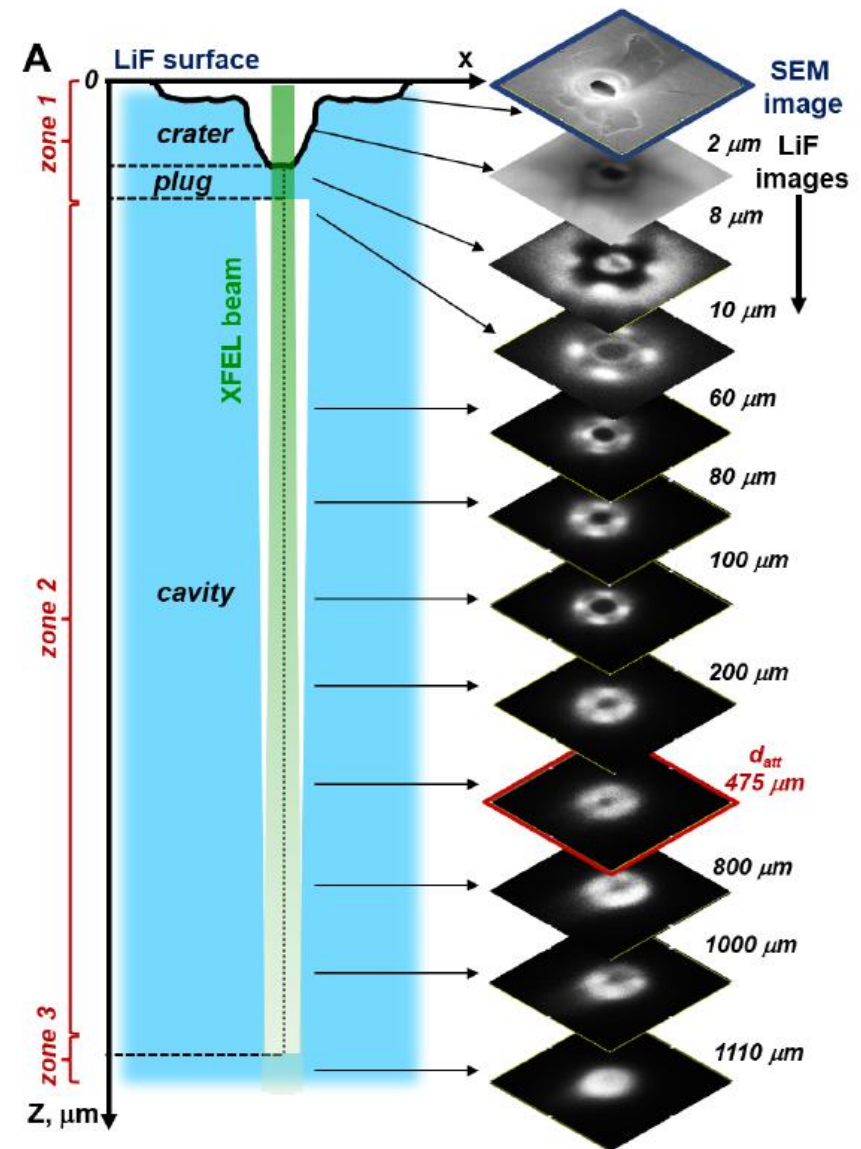
Three zones

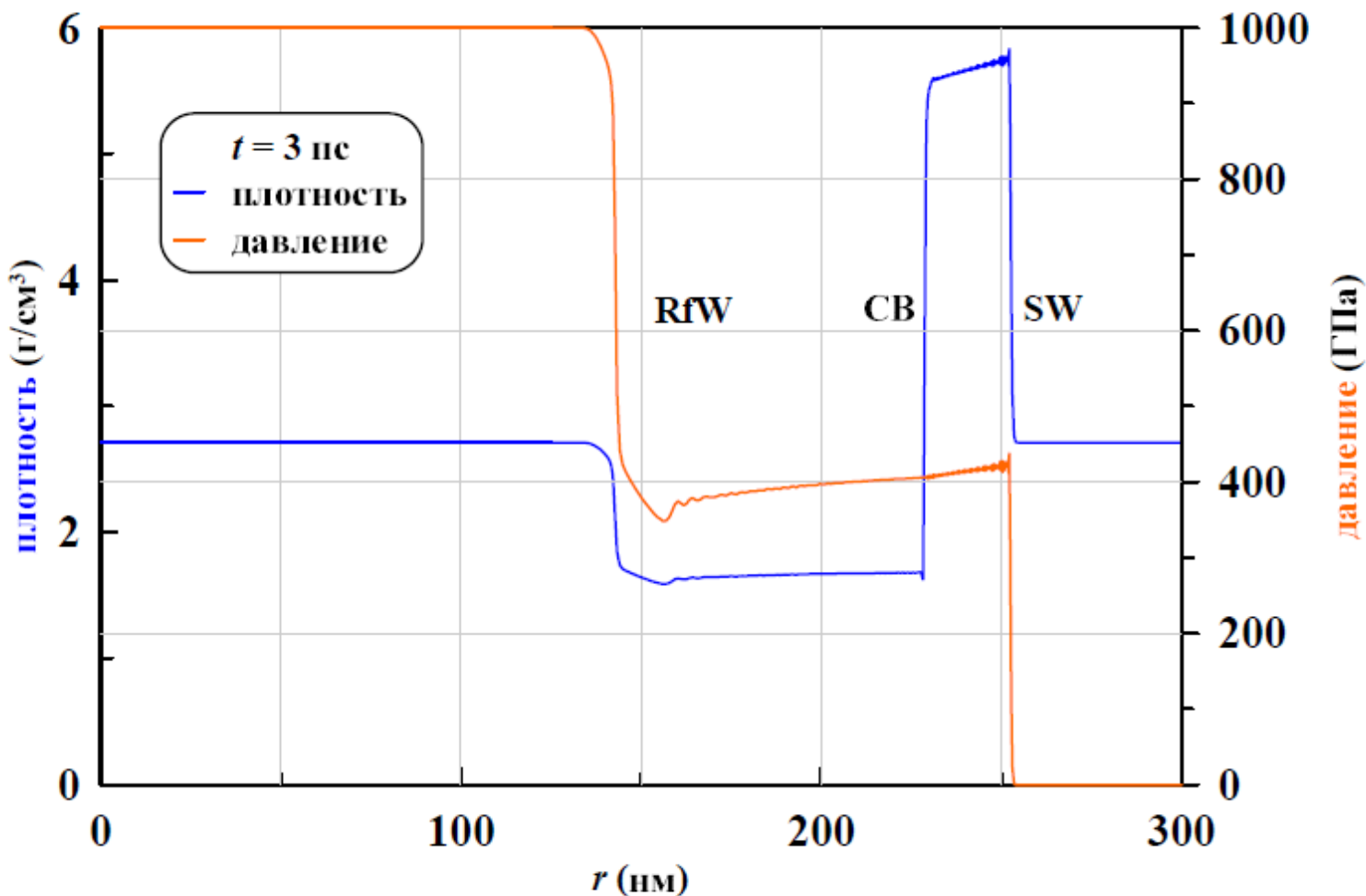
The deepest third zone is extremely unusual and interesting.

The empty long channel is finished.

But not due to similar in our community spallation like phenomena but...

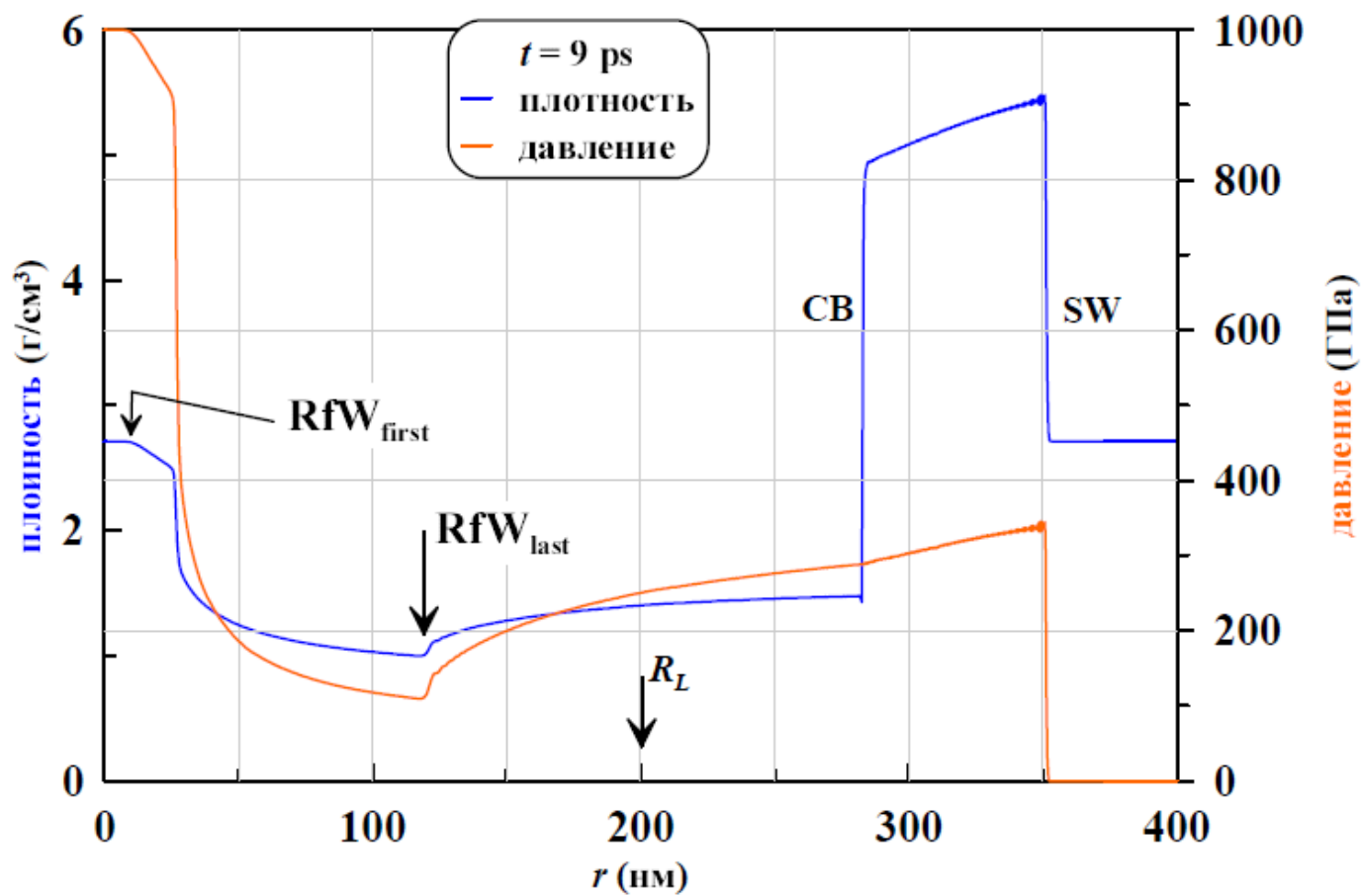
See report which will be given by Zhakhovsky:
 Zhakhovsky, Grigoryev, Perov E.
 “Formation of a cylindrical cavity in LiF crystal by X-ray pulse”





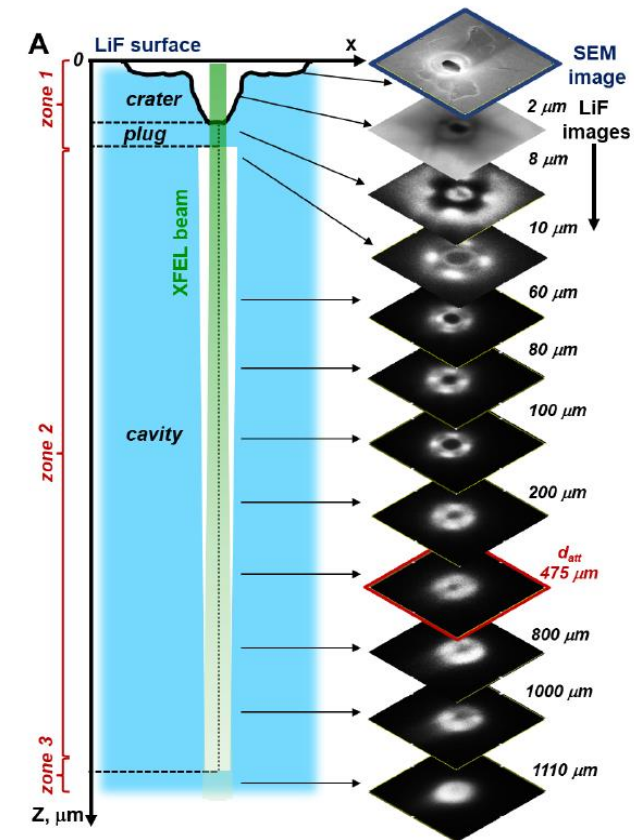
Распад разрыва
в цилиндрической
геометрии

Рисунок 1. Профили плотности (синяя кривая) и давления (оранжевая кривая) в момент времени 3 пс. Распад разрыва, расширение высокоэнтропийного цилиндра (его граница СВ), излучение УВ (SW) и волны разрежения (RfW). Начальная координата края горячего цилиндра $R_L = 200$ нм.



Расчет поясняет, каким образом происходит отбрасывание кф ЛиФ от оси пучка и образуется длинная полость - прокол

Рисунок 2. Профили плотности (синяя кривая) и давления (оранжевая кривая) в момент времени 9 пс. Стрелками RfW_{first} и RfW_{last} показаны края волны разрежения (ВР), распространяющейся в сторону оси $r = 0$. Передний фронт ВР RfW_{first} подошел вплотную к центру. Его координата равна 10.3 нм, т.е. 5% от начального радиуса цилиндра R_L . Этот фронт движется со скоростью звука $c_{sh} = 19.7$ км/с в горячем невозмущенном веществе. В момент 9.52 пс характеристика RfW_{first} достигает центра — начинается отражение характеристик ВР от центра.



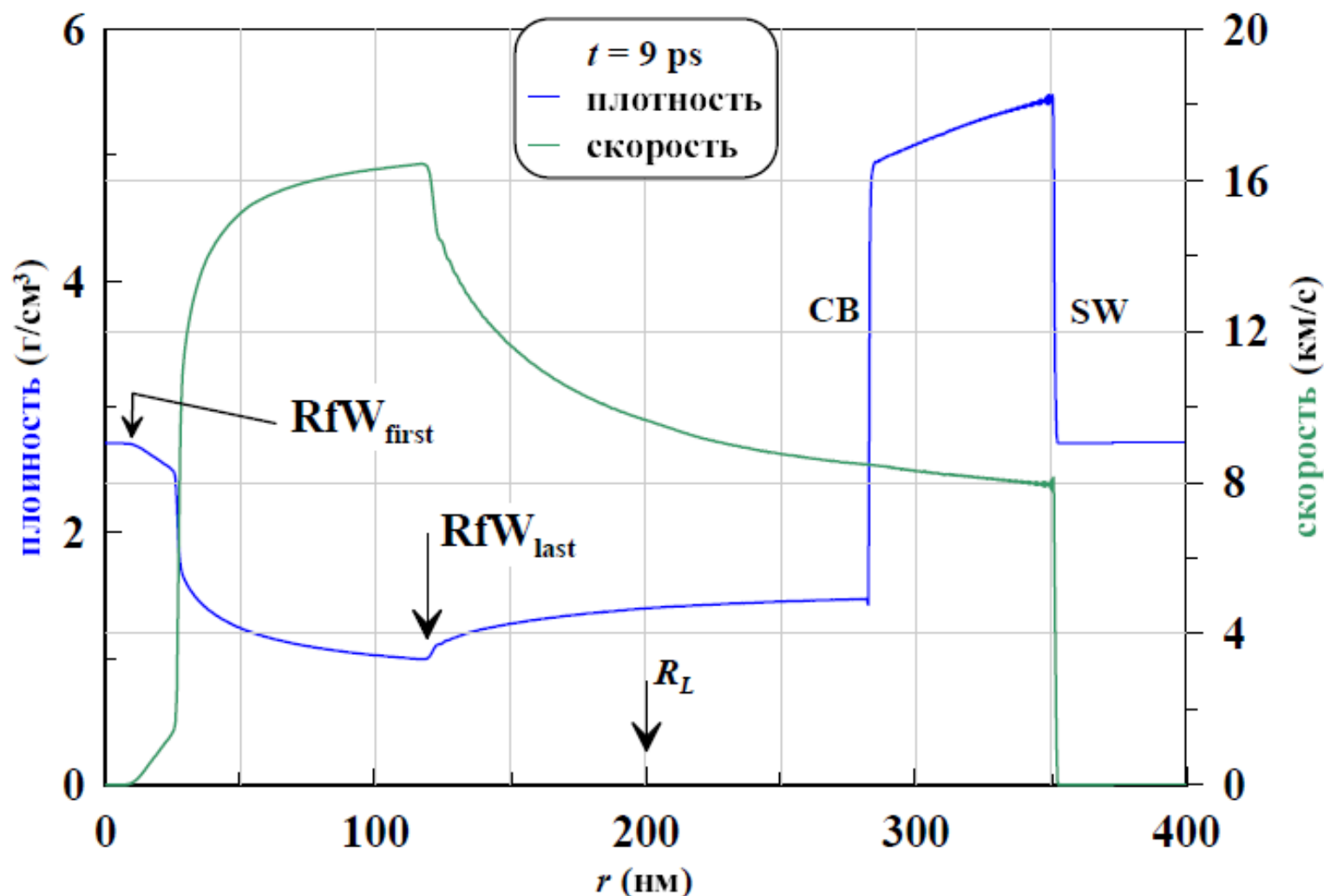


Рисунок 3. Профили плотности (синяя кривая) и радиальной скорости (зеленая кривая) в момент времени 9 пс. Стрелки перенесены с рисунка 2. Удивительно, гидродинамическая скорость на бегущей характеристике RfW_{last} растет со временем и в момент 9 пс составляет величину 16.4 км/с, превышающую скорость УВ 15.7 км/с в этот момент.

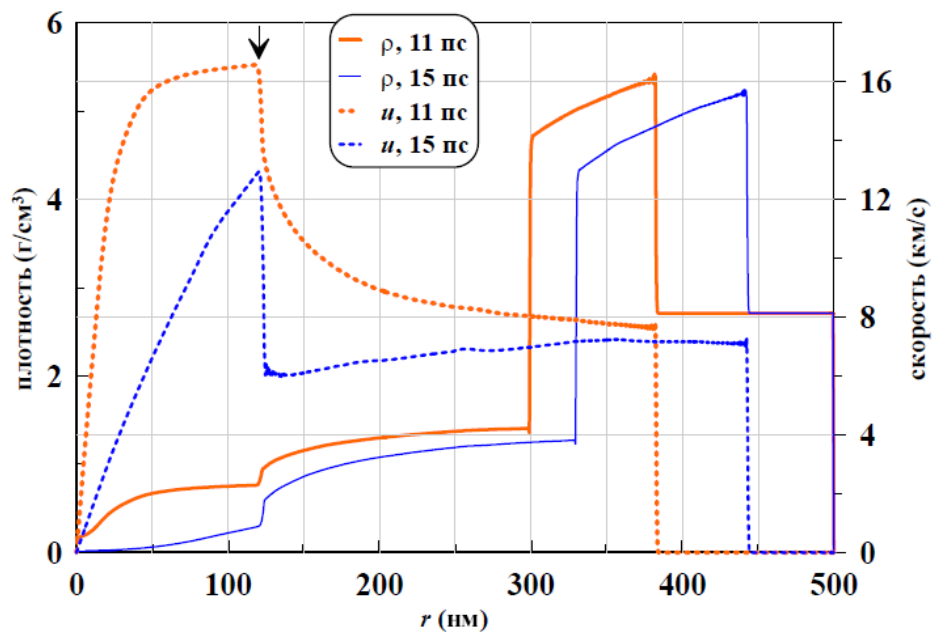


Рисунок 4. Сравнение плотностей и скоростей в моменты времени 11 и 15 пс.

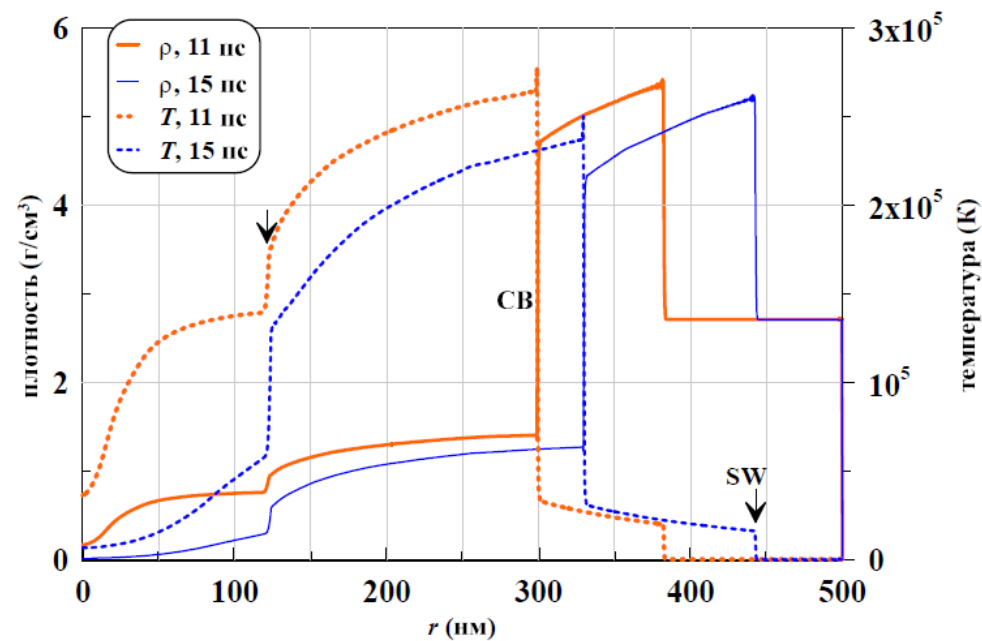


Рисунок 5. Сравнение плотностей и температур в моменты времени 11 и 15 пс.

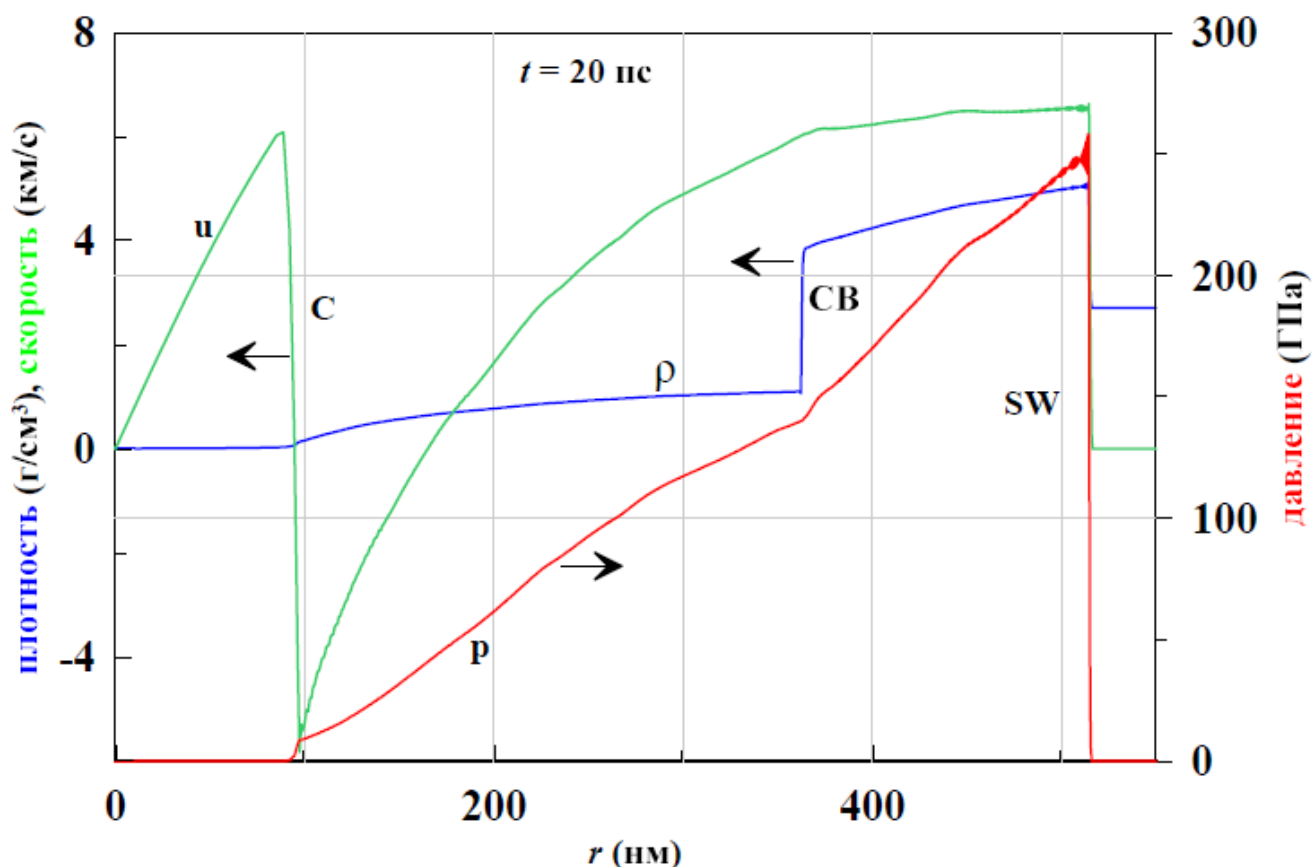


Рисунок 7. Профили плотности (синяя кривая), давления (красная кривая) и скорости (зеленая кривая) на момент времени 20 пс. Горизонтальные стрелки у кривых указывают, какая кривая к какой оси ординат относится. Перечислим порядок следования характерных участков слева направо от оси к периферии. Имеются 1) область соударения ветров С, 2) контакт СВ и 3) ударная волна SW. В центральной области (левее точки С) плотность и давление падают практически до нуля. Отметим смену знака скорости на краю трансформированной пробки, т.е. правее зоны соударения С. Теперь эта скорость направлена к центру симметрии.

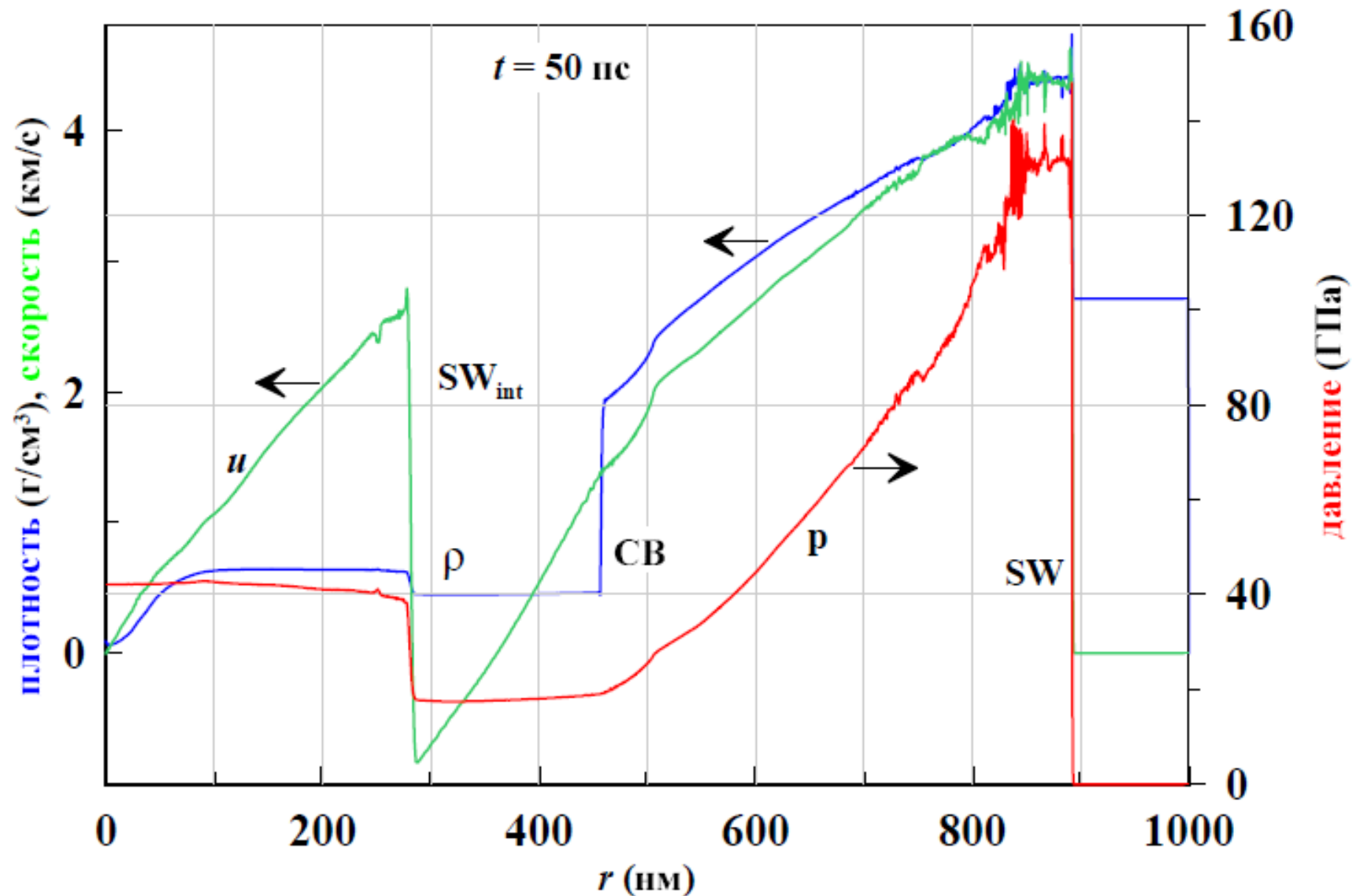


Рисунок 8. Те же профили и те же горизонтальные стрелки, что и на предыдущем рисунке 7, но теперь в момент 50 пс. Из центра идет ударная волна SW_{int} .



$$\frac{\partial r(r^0, t)}{\partial t} = v(r^0, t), \quad (3)$$

$$\rho r \frac{\partial r(r^0, t)}{\partial r^0} = \rho_0 r^0, \quad (4)$$

$$\frac{\partial v(r^0, t)}{\partial t} = -\frac{1}{\rho_0 r^0} \frac{\partial(r P)}{\partial r^0}, \quad P = P_e + P_i, \quad (5)$$

$$\begin{aligned} \frac{\partial E_e(x^0, t)}{\partial t} = & \frac{1}{\rho_0 r^0} \frac{\partial}{\partial r^0} \left(\frac{\kappa \rho r}{\rho_0} \frac{\partial T_e}{\partial r^0} \right) \\ & - \alpha_\rho (T_e - T_i) + \frac{Q(r^0, t)}{\rho} - \frac{P_e}{\rho_0 r^0} \frac{\partial(vr)}{\partial r^0}, \end{aligned} \quad (6)$$

$$\frac{\partial E_i(r^0, t)}{\partial t} = +\alpha_\rho (T_e - T_i) - \frac{P_i}{\rho_0 r^0} \frac{\partial(vr)}{\partial r^0}, \quad (7)$$

В начальный момент $t = 0$ лагранжева и эйлерова координаты совпадают ($r^0 = r$.) В начальный момент вещество покоится. Плотность однородна и равна ρ_0 . Давление и температура внутри цилиндра $r^0 = r < R_L$ равны 10 Мбар и 550 кК. Нас будут интересовать времена, большие по сравнению с временем электрон-ионной релаксации, поэтому будем использовать одготемпературный ($(T_e = T_i)$) подход: соответственно уравнение (7) использоваться не будет, $P_e = 0, E_e = 0$.

Дорогие участники
конференции ЗНЧ-2025
спасибо, что выслушали

